J. Indian Inst. Sci., Jan.–Feb. 1996, 76, 59–72.

Bore optimization for rotating hollow shallow shell

K. R. Y. SIMHA[†], RAJEEV JAIN[‡] AND K. RAMACHANDRA[‡]
[†]Department of Mechanical Engineering, Indian Institute of Science, Bangalore 560 012
[‡]Gas Turbine Research Establishment, Bangalore 560 093.

Received on November 1, 1995.

Abstract

This paper is concerned with the minimization of the hoop stress at the bore due to the combined membrane and bending action for a rotating hollow shallow shell. A novel iterative scheme is developed to apply the free boundary conditions at the rim and the bore. Hoop stress concentration factors are presented for 16 different combinations of shell thickness and rim radius to arrive at the optimum bore size. The results also reveal the importance of the shell thickness for an optimum bore size to ensure a reasonably uniform hoop stress distribution along the radius of the shell.

Keywords: Rotating discs, elasticity, circular bore, hoop stress, bore optimization.

Notation

E : Young's modulus of elasticity
ν : Poisson's ratio
a : shallow shell radius
r_b : bore radius
r_c : maximum radial distance from axis of rotation
ω : angular velocity radian/s
p : load intensity in normal direction = $\rho\omega^2h^2/a$
p_r : load intensity in meridional direction $\approx \rho\omega^2h(1-r^2/a^2)$
Ω : body force potential = $-\int p_r\, dr$
F : stress function
Δ : $d^2/dr^2 + (1/r)d/dr$
l : characteristic length
x : dimensionless parameter = r/l
D : $Eh^3/12(1-\nu^2)$
N_r : membrane force in radial direction
N_θ : membrane force in tangential direction
h : thickness of the rotating shell $h' = dh/dr$, $h'' = d^2h/dr^2$
M_r : bending moment in radial direction
M_θ : bending moment in tangential direction
ρ : mass density
w : normal deflection $w' = dw/dr$, $w'' = d^2w/dr^2$

1. Introduction

Design of rotating discs for turbine applications demands a thorough appreciation of advanced theories of elasticity. Often discs become bent due to axial deformation caused by differential gas pressure as well as axial loads acting on the blades. As a consequence, the discs assume the shape of a shallow shell. If the associated flexural stress and deflection exceed critical values the situation becomes dangerous. An earlier paper[1] analysed the stresses and displacements in a rotating shallow shell of variable thickness. The effect of a circular bore was not considered in the previous work. The main thrust of this paper is on the optimization of the bore size for a constant thickness shell. Minimizing the hoop stress at the bore of a rotating shallow shell constitutes the theme of optimization. It is well known that the hoop stress is doubled when a small hole is drilled at the centre of a rotating flat disc[2]. This remarkable result continues to hold for a rotating shallow shell for both stress (N_θ) and moment (M_θ) resultants. Engineering design, however, generally requires a bore size which is a considerable fraction of the outer disc diameter. Earliest reference to this aspect of turbine disc design suggests a ratio of 1/5[3]. This suggestion has been widely followed, although there appears to be no documented theoretical evidence. In fact, the optimum bore size for a flat rotating disc is achieved in the limit the bore shrinks to a point. For a flat disc, the hoop stress concentration factor defined with respect to the stress at the centre of a solid disc monotonically increases with the bore size according to equation $K_n = 2+2(1-\nu)r_b^2/(3+\nu)r_c^2$. As will be shown in this paper, the behaviour of a rotating shallow shell with regard to the hoop stress at the bore is interestingly different from that of a flat disc.

The hoop stress concentration factor due to the membrane action in a rotating shallow shell initially decreases with increasing bore size reaching a minimum before increasing monotonically as in the case of a flat disc. This surprising result presents a valuable insight for optimal design. What is more surprising is the fact that the optimum ratio r_c/r_b is around 1/5, or quite close to engineering practice as for as N_θ is concerned. However, the net hoop stress concentration factor (K_n) comprises both membrane (K_m) and bending effect (K_b). The net hoop stress concentration factor is not minimized when r_c/r_b is around 1/5, but depends on the size and thickness of the rotating shell as addressed in this paper.

Results are presented for the hoop stress concentration factor normalised with respect to a solid shell of the same configuration. All the results have also been verified with FEM calculations using a commercial software, not included in this paper. Optimization is then discussed based on $K_n = \sigma_\theta^{\text{hollow}}/\sigma_\theta^{\text{solid}}$. Stress variation along the radius of the shell is also examined for the optimized cases to assess the effectiveness of optimization based on the bore stress. A novel iterative scheme of applying the boundary condition for rotating hollow shells is also proposed in this paper.

2. Optimization problem

The design optimization is discussed with respect to Fig. 1. For given values of a, h, r_c, the problem is to determine the optimum value of the bore radius r_b that will minimize

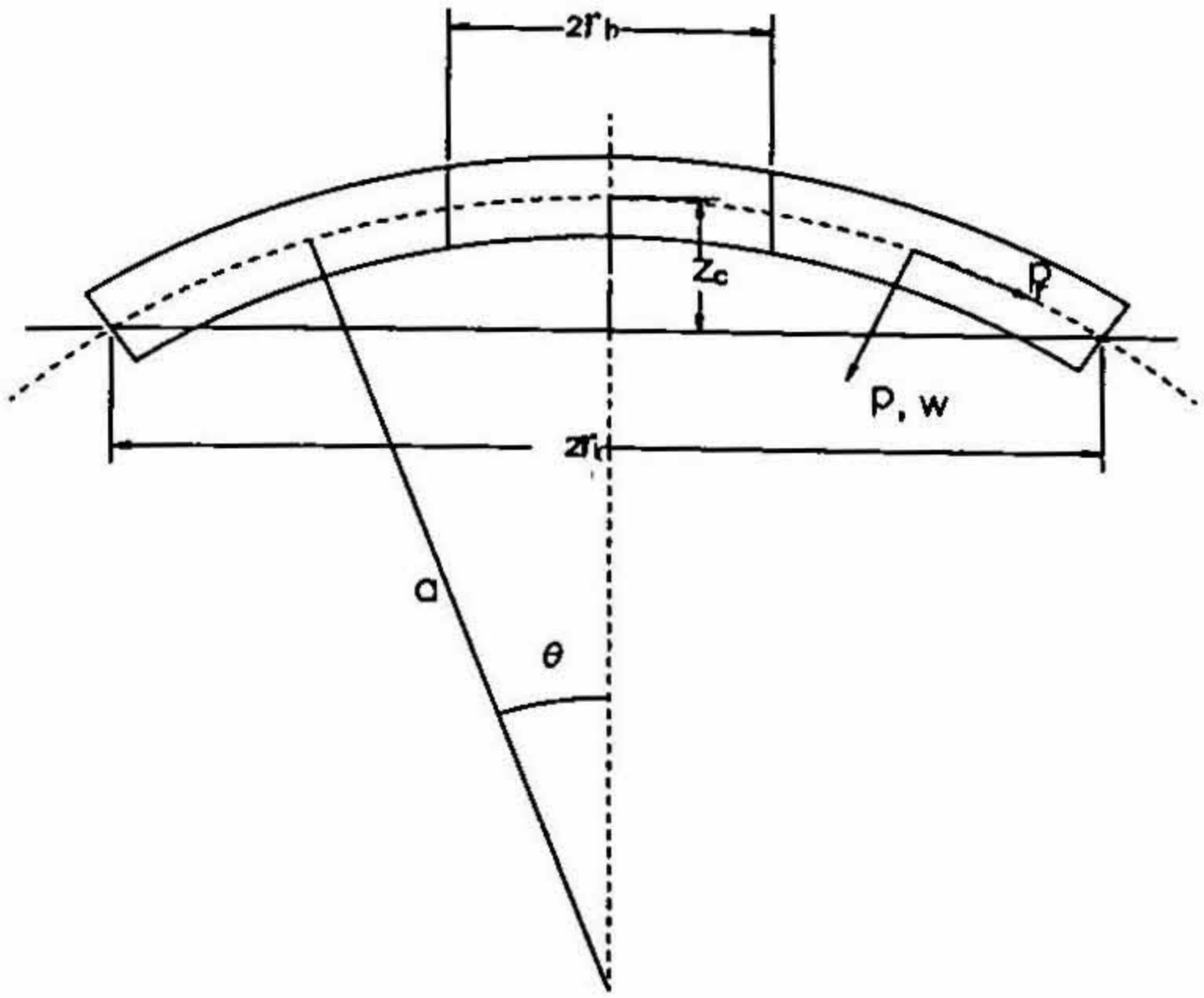

FIG. 1 Rotating shallow disc configuration.

the hoop stress concentration at the bore. We have to also examine how uniform the resulting hoop stress variation is along the radius from the bore to the rim of the shallow shell. We follow the general procedure outlined in Flügge[4], and Timoshenko and Woinowosky–Krieger[5] for constant thickness shells, and extended to variable thickness shells by the authors.

2.1. *Problem formulation*

The governing differential equations are

$$\Delta\Delta F + \frac{Eh}{a}\Delta w - \frac{h'}{h}\left(2F''' + \frac{(2-\nu)}{r}F'' - \frac{F'}{r^2}\right) - \frac{h''}{h}\left(F'' - \frac{\nu}{r}F'\right) + 2\left(\frac{h'}{h}\right)^2\left(F'' - \frac{\nu}{r}F'\right)$$

$$= -(1-\nu)\Delta\Omega + \frac{h'}{h}\left(2(1-\nu)\Omega' + (1-\nu)\frac{\Omega}{r}\right) + \frac{h''}{h}(1-\nu)\Omega - 2\left(\frac{h'}{h}\right)^2(1-\nu)\Omega$$

$$\Delta\Delta w - \frac{1}{aD}\Delta F + \frac{3h'}{h}\left(2w'' + \frac{(2+\nu)}{r}w'' - \frac{w'}{r^2}\right) + \frac{3h''}{h}\left(w'' + \frac{\nu}{r}w'\right)$$

$$+ 6\left(\frac{h'}{h}\right)^2\left(w'' + \frac{\nu}{r}w'\right) = \frac{2\Omega}{aD} + \frac{p}{D}. \tag{1}$$

In the case of constant thickness shell, eqns(1) reduce to:

$$\Delta\Delta F + \frac{Eh}{a}\Delta w = -(1-\nu)\Delta\Omega; \tag{2}$$

$$\Delta\Delta w - \frac{1}{Da}\Delta F = \frac{p}{D} + \frac{2\Omega}{Da}. \tag{3}$$

The integration of simultaneous equations, (2) and (3), can be carried out by multiplying eqn (2) by a factor $-\lambda$ and adding the result to eqn (3). This yields

$$\Delta\Delta(w - \lambda F) - \lambda\left(\frac{Eh}{a}\right)\Delta\left(w + \frac{F}{\lambda hDE}\right) = \lambda(1-\nu)\Delta\Omega + \frac{p}{D} + \frac{2\Omega}{Da}. \tag{4}$$

2.2. *Homogeneous solution* ($p = \Omega = 0$)

Stipulating $\lambda = -1/\lambda h, DE$ yields

$$\Delta\Delta\Psi - \frac{\lambda Eh}{a}\Delta\Psi = 0, \tag{5}$$

where $\Psi = w - \lambda F$ and $\lambda = i/Eh^2\sqrt{12(1-\nu^2)}$. The homogeneous solution for the above equation is $\Psi = \Psi_1 + \Psi_2$, where

$$\Psi_1 = A_1 + A_2 \log x$$

$$\Psi_2 = A_3(\text{ber } x + i \text{ bei } x) + A_4(\text{ker } x + i \text{ kei } x). \tag{6}$$

The functions ber, bei, ker and kei are Bessel's functions for imaginary arguments[6]. Assuming $A_i = a_i + i\,b_i$ where a_i, b_i are real constants to be determined, we get

$$w = a_1 + a_2 \log x + a_3 \text{ber } x - b_3 \text{bei } x + a_4 \text{ ker } x - b_4 \text{kei } x$$

$$F = -\frac{Eh^2}{\sqrt{12(1-\nu^2)}}(b_1 + b_2 \log x + b_3 \text{ber } x + b_4 \text{ ker } x + a_3 \text{bei } x + a_4 \text{kei } x). \tag{7}$$

2.3. *Particular solution*

The particular integral of (5) is taken as

$$\Psi = (Q_1 + \lambda R_1)r^2 + (Q_2 + \lambda R_2)r^4 + (Q_3 + \lambda R_3)r^6$$

where

$$Q_1 = \frac{-\rho\omega^2 a}{2E}\left(\overline{\nu+3} - \frac{2h^2}{a^2(1+\nu)}\right) \qquad R_1 = -\frac{2\rho\omega^2(1+\nu)D}{E}$$

$$Q_2 = \frac{\rho\omega^2(1+\nu)}{8aE} \qquad R_2 = -\frac{\rho\omega^2 h}{8}\left(1 - \frac{h^2}{2a^2(1+\nu)}\right)$$

$$Q_3 = -\frac{\rho\omega^2(1-\nu)}{48Ea^3} \qquad R_3 = \frac{\rho\omega^2 h}{144a^2}. \tag{8}$$

Hence, the complete solution is

$$w = a_1 + a_2 \log x + a_3 \text{ber } x + a_4 \ker x - b_3 \text{bei } x - b_4 \text{kei } x + Q_1 r^2 + Q_2 r^4 + Q_3 r^6$$

$$F = -\frac{Eh^2}{\sqrt{12(1-\nu^2)}} (b_1 + b_2 \log x + b_3 \text{ber } x + b_4 \ker x + a_3 \text{bei } x + a_4 \text{kei } x)$$

$$-R_1 r^2 - R_2 r^4 - R_3 r^6. \tag{9}$$

Of the eight constants appearing above, b_1 can be omitted as it will not produce any stress, whereas constant a_2 can be omitted[2] because of multivalued contribution to the displacement u_θ; further, b_2 can be absorbed into b_4, leaving only five constants.

Boundary conditions $N_r, M_r, = 0$ @ $r = r_b, r_c$ and $w = 0$ @ $r = r_b$ determine a_1, a_2, a_3, b_3, and b_4 as follows

$$\begin{bmatrix} K_{11} & K_{12} & K_{13} & K_{14} & K_{15} \\ K_{21} & K_{22} & K_{23} & K_{24} & K_{25} \\ K_{31} & K_{32} & K_{33} & K_{34} & K_{35} \\ K_{41} & K_{42} & K_{43} & K_{44} & K_{45} \\ K_{51} & K_{52} & K_{53} & K_{54} & K_{55} \end{bmatrix} \begin{bmatrix} a_1 \\ a_3 \\ a_4 \\ b_3 \\ b_4 \end{bmatrix} = \begin{bmatrix} C_1 \\ C_2 \\ C_3 \\ C_4 \\ C_5 \end{bmatrix} \tag{10}$$

where

$$K_{11} = 1 \quad K_{12} = \text{ber } x_b \quad K_{13} = \ker x_b$$

$$K_{21} = 0 \quad K_{22} = \frac{\text{bei}' x_b}{x_b} \quad K_{23} = \frac{\text{kei}' x_b}{x_b}$$

$$K_{31} = 0 \quad K_{32} = \frac{\text{bei}' x_c}{x_b} \quad K_{33} = \frac{\text{kei}' x_c}{x_c}$$

$$K_{41} = 0 \quad K_{42} = \left(\text{ber}'' x_b + \nu \frac{\text{ber}' x_b}{x_b} \right) \quad K_{43} = \left(\ker'' x_b + \nu \frac{\ker' x_b}{x_b} \right)$$

$$K_{51} = 0 \quad K_{52} = \left(\text{ber}'' x_c + \nu \frac{\text{ber}' x_c}{x_c} \right) \quad K_{53} = \left(\ker'' x_c + \nu \frac{\ker' x_c}{x_c} \right)$$

$$K_{14} = -\text{bei } x_b \quad K_{15} = -\text{kei } x_b$$

$$K_{24} = \frac{\text{ber}' x_b}{x_b} \quad K_{25} = \frac{\ker' x_b}{x_b}$$

$$K_{34} = \frac{\text{ber}' x_c}{x_c} \quad K_{35} = \frac{\ker' x_c}{x_c}$$

$$K_{44} = -\left(\text{bei}''\, x_b + \nu \frac{\text{bei}'\, x_b}{x_b}\right) \quad K_{45} = -\left(\text{kei}'' x_b + \nu \frac{\text{kei}' x_b}{x_b}\right)$$

$$K_{54} = -\left(\text{bei}''\, x_c + \nu \frac{\text{bei}'\, x_c}{x_c}\right) \quad K_{55} = -\left(\text{kei}''\, x_c + \nu \frac{\text{kei}'\, x_c}{x_c}\right)$$

and

$$C_1 = -Q_1 r_b^2 - Q_2 r_b^4 - Q_3 r_b^6$$

$$C_2 = -\frac{a}{Eh}\left(2R_1 + 4R_2 r_b^2 + 6R_3 r_b^4 - \Omega\right)$$

$$C_3 = -\frac{a}{Eh}\left(2R_1 + 4R_2 r_c^2 + 6R_3 r_c^4 - \Omega\right)$$

$$C_4 = -\left(2Q_1(1+\nu) + 4Q_2(3+\nu) r_b^2 + 6Q_3(5+\nu) r_b^4\right) l^2$$

$$C_5 = -\left(2Q_1(1+\nu) + 4Q_2(3+\nu) r_c^2 + 6Q_3(5+\nu) r_c^4\right) l^2.$$

2.4. *Stress-doubling effect of small hole*

For a solid shallow disc[8], only three constants a_1, a_2 and b_3 are involved as follows

$$\begin{bmatrix} K_{11} & K_{12} & K_{14} \\ K_{31} & K_{32} & K_{34} \\ K_{51} & K_{52} & K_{54} \end{bmatrix} \begin{bmatrix} a_1^* \\ a_3^* \\ b_3^* \end{bmatrix} = \begin{bmatrix} C_1 \\ C_3 \\ C_5 \end{bmatrix} \tag{11}$$

where

$$K_{11} = 1 \quad K_{12} = 1.0 \quad K_{14} = 0.0$$

$$K_{31} = 0 \quad K_{32} = \frac{\text{bei}'\, x_c}{x_c} \quad K_{34} = \frac{\text{ber}'\, x_c}{x_c}$$

$$K_{51} = 0 \quad K_{52} = \left(\text{ber}''\, x_c + \nu \frac{\text{ber}'\, x_c}{x_c}\right) \quad K_{54} = -\left(\text{bei}''\, x_c + \nu \frac{\text{bei}'\, x_c}{x_c}\right).$$

Solving (10) and (11) shows that both N_θ and M_θ are doubled when a small hole is made in a rotating solid shallow shell.

2.5. *Iterative solution*

A novel iterative solution is explained in this section to extract the constants a_1 to b_4 by taking advantage of the values of a_1, a_3 and b_3 for a solid disc. It is observed that the

values of constants a_1, a_3 and b_3 for the hollow rotating shell are quite close to the corresponding values for a solid shell. The solid shell values can therefore be used for the hollow shell problem in the first iteration to deterime a_4 and b_4. The new values of a_4 and b_4 are used in the second iteration to determine a_1, a_3 and b_3. This process is continued until the results converge. Figure 2 shows the flowchart. The main advantage of using this iterative scheme lies in solving sets of (3×3) and (2×2) linear equations instead of the more complicated (5×5) linear equation (10). Rapid convergence is noted for all the cases investigated. A typical convergence history of the constants a_1,... b_4 is shown in Fig. 3 for the case of $r_b = 50$ mm, $r_c = 200$ mm, $h = 10$ mm, $a = 1000$ mm. To highlight the concept of the approach, this iterative scheme is demonstrated for the simple case of a flat rotating disc of inner radius r_b and outer radius r_c. The radial stress is

$$\sigma_r = C_1 + \frac{C_2}{r^2} - \frac{3+\nu}{8}\rho\omega^2 r^2. \tag{12}$$

Denoting $(3+\nu)\rho\omega^2/8 = K$, for a solid disc $C_2^{[0]} = 0$ and $C_1^{[0]} = Kr_c^2$ and using the above value of $C_1^{[0]}$ in eqn (12) and applying the free boundary condition at the inner boundary, we get

$$C_2^{[1]} = -Kr_b^2 r_c^2\left[1-\left(\frac{r_b}{r_c}\right)^2\right].$$

Repeating this process on the outer boundary, we get

$$C_1^{[1]} = K\left(r_b^2 + r_c^2\right)\left[1-\frac{r_b^2}{r_b^2+r_c^2}\left(\frac{r_b}{r_c}\right)^2\right].$$

The corresponding value of C_2 using the inner boundary is

$$C_2^{[2]} = -Kr_b^2 r_c^2\left[1-\left(\frac{r_b}{r_c}\right)^4\right].$$

Using $C_2^{[2]}$ and the outer boundary, we complete the second iteration

$$C_1^{[1]} = K\left(r_b^2 + r_c^2\right)\left[1-\frac{r_b^2}{r_b^2+r_c^2}\left(\frac{r_b}{r_c}\right)^4\right].$$

Continuing this process, after n iterations, we get

$$C_2^{[n]} = -Kr_b^2 r_c^2\left[1-\left(\frac{r_b}{r_c}\right)^{n+2}\right]$$

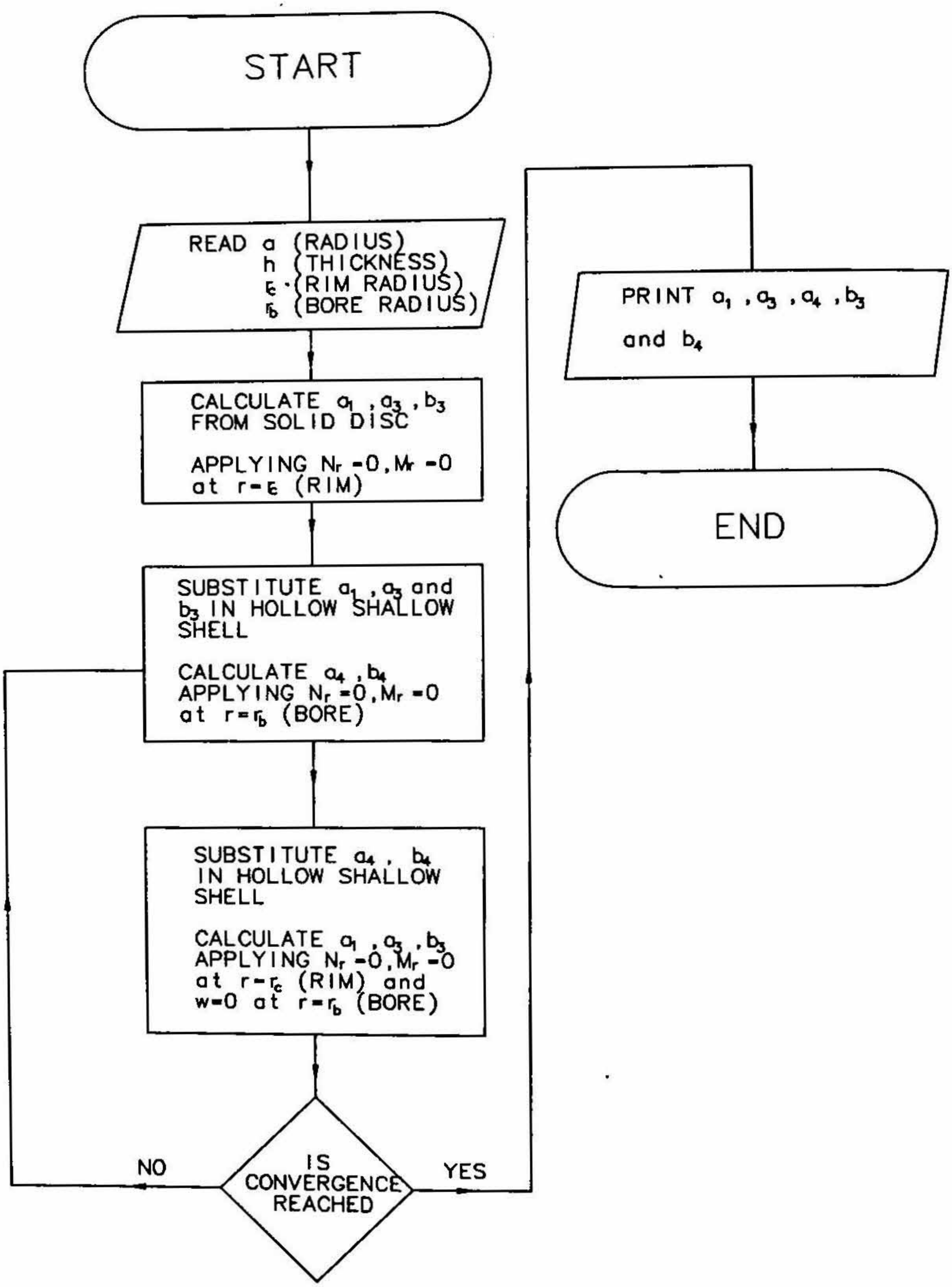

FIG. 2. Flow chart for iterative solution.

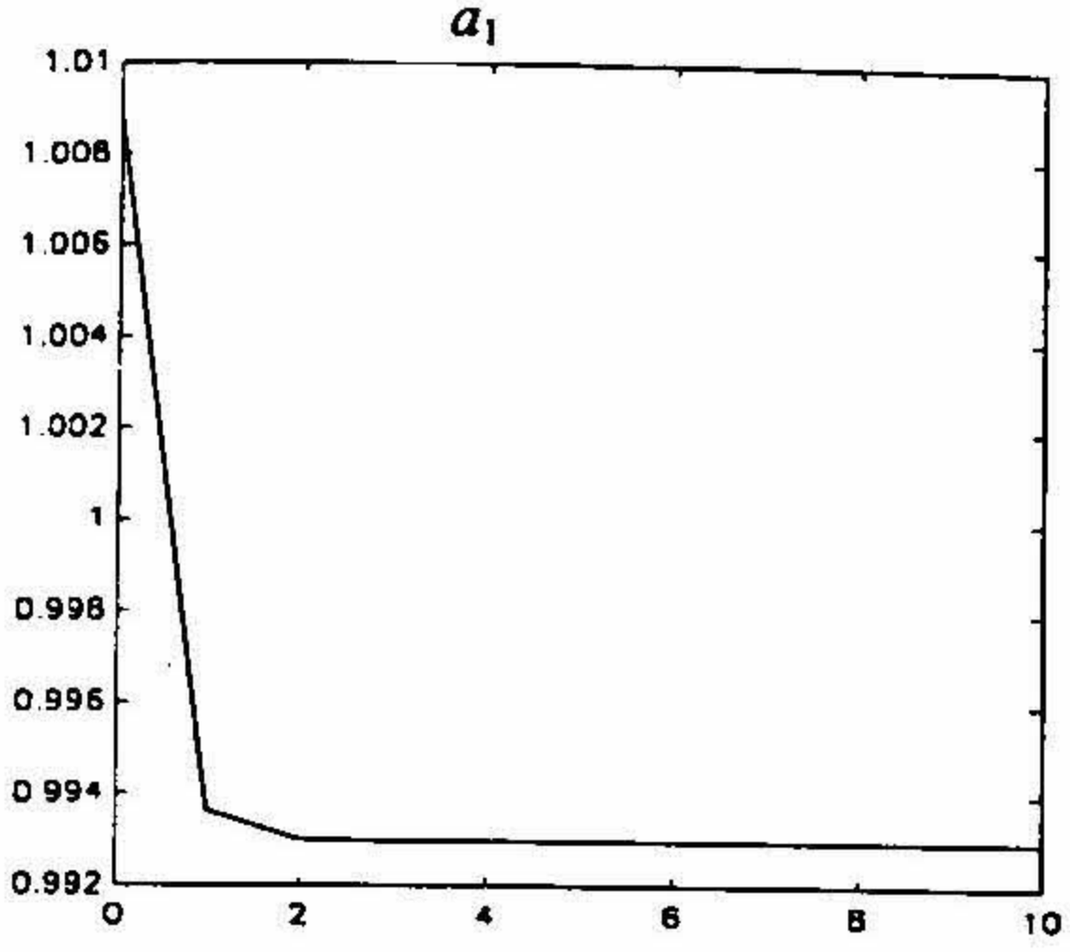

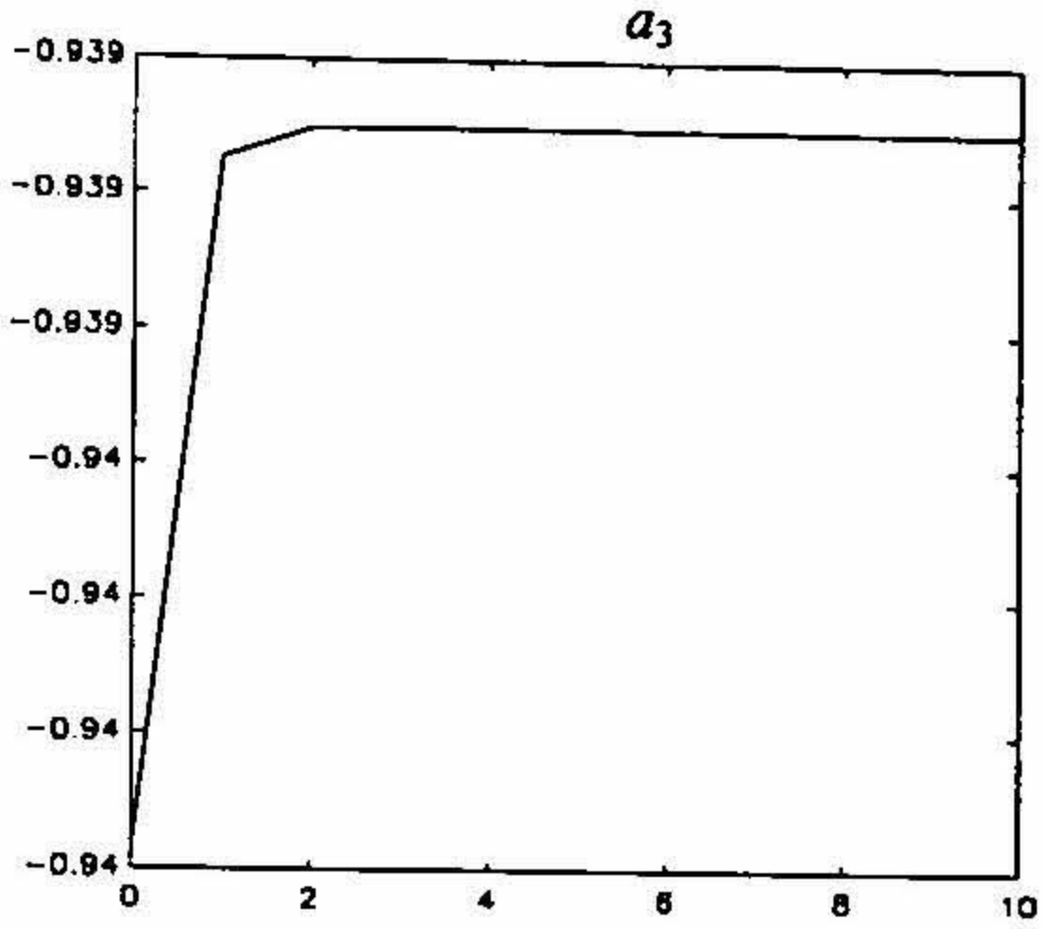

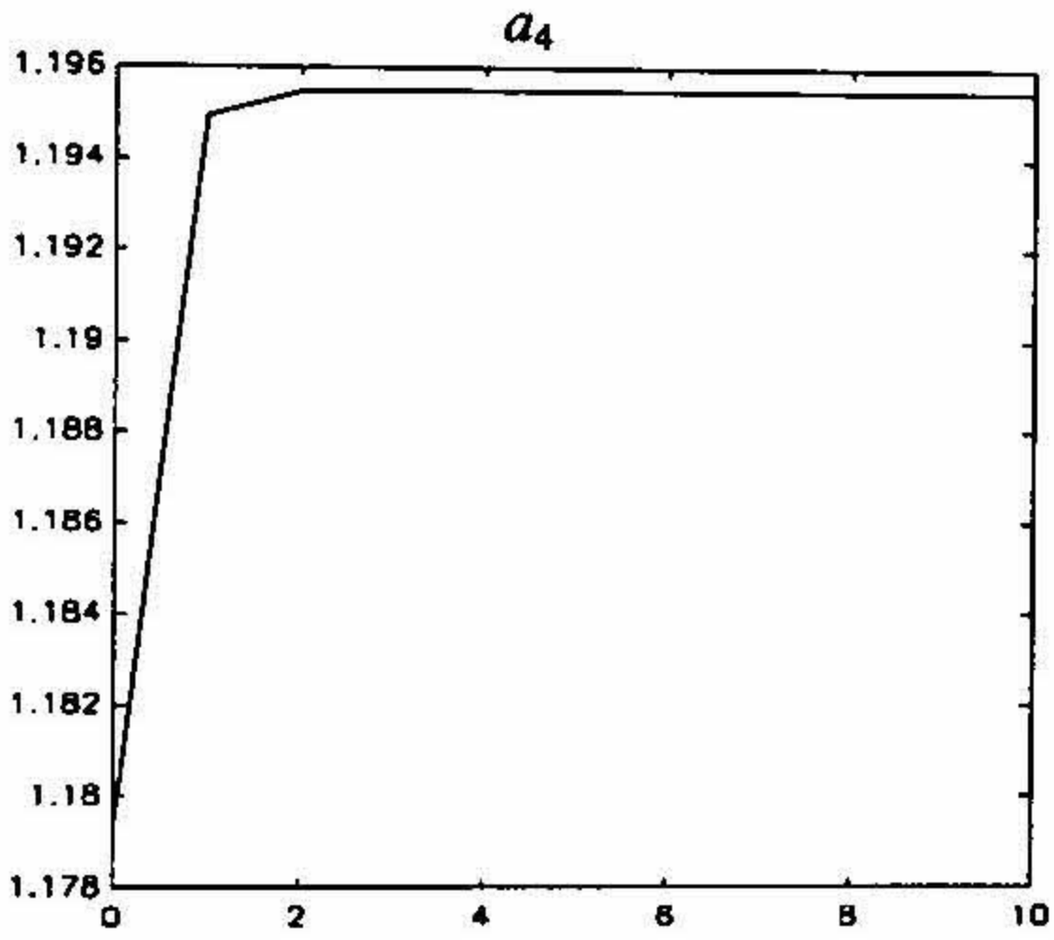

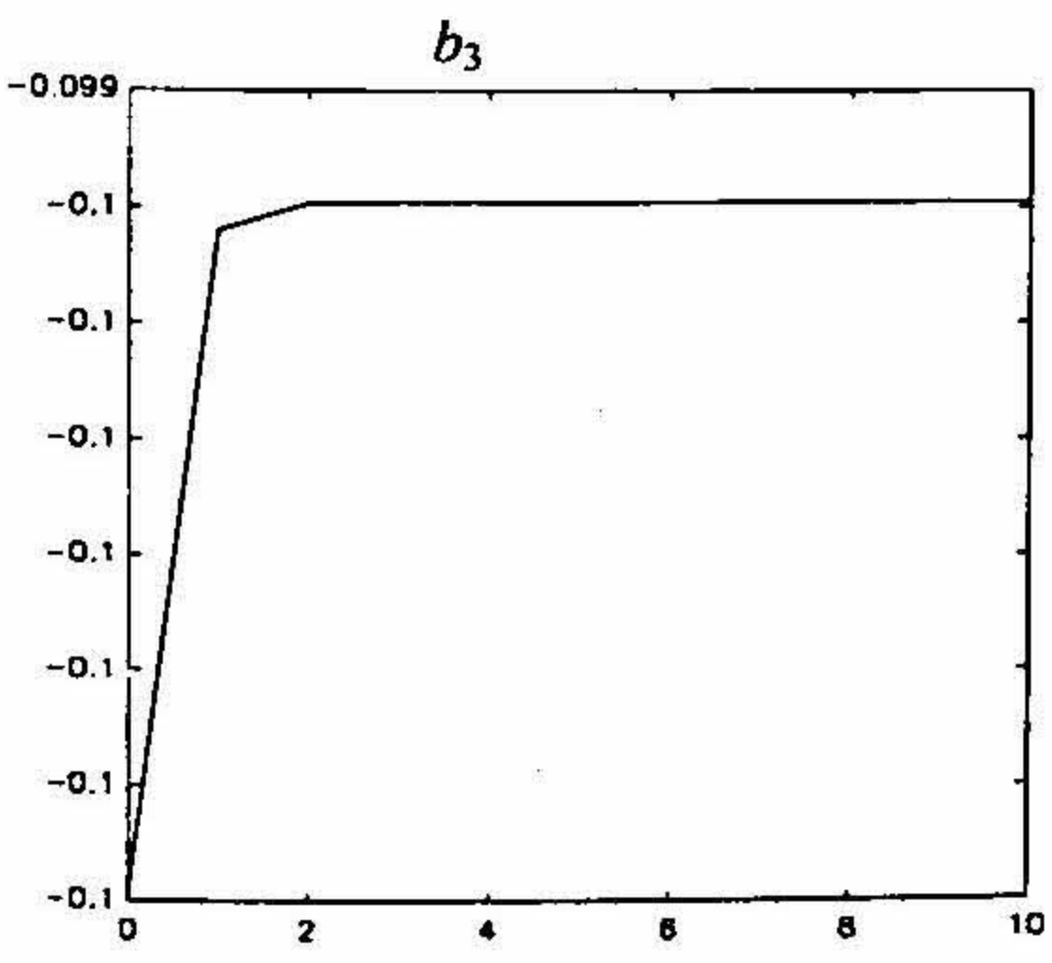

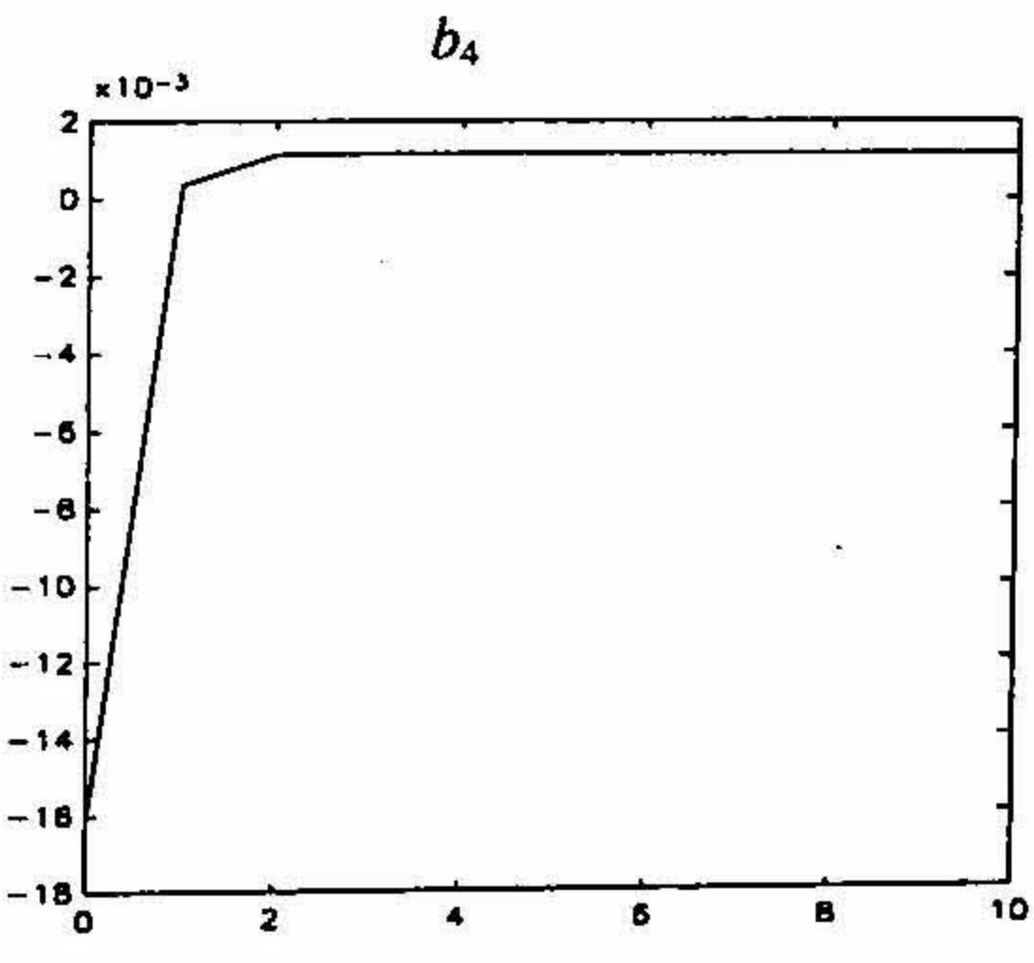

FIG. 3. Variation of constants a_1, a_2, a_3, and b_3 and b_4 with number of iterations.

$$C_1^{[n]} = K\left(r_b^2 + r_c^2\right)\left[1 - \frac{r_b^2}{r_b^2 + r_c^2}\left(\frac{r_b}{r_c}\right)^{n+2}\right].$$

Since $r_b/r_c < 1$, the solution converges to the exact result

$$C_1 = K\left(r_b^2 + r_c^2\right);$$
$$C_2 = -Kr_b^2 r_c^2.$$

This proves the validity of the iterative procedure.

3. Results

Calculations are performed for four different rim radii r_c = 180, 200, 220 and 240 mm, and for four different shell thicknesses h = 8, 10, 11 and 12 mm. In all the cases, the sagitta is held constant at 20 mm. The specific gravity and rotational speed of the shell are taken as 7.85 and 17,000 rpm, respectively. All the stresses are normalized with respect to the hoop stress at the centre of the corresponding *solid shallow shell*. These stresses are calculated as

$$\sigma_m = -\frac{Ea_3}{2a} + \frac{\rho\omega^2 h^2}{3(1-\nu)} \text{ (membrane)}$$

$$\sigma_b = \frac{3E(1+\nu)b_3}{\sqrt{12\left(1-\nu^2\right)}a} + \frac{\rho\omega^2 ah}{2(1-\nu)}\left(\nu + 3 - \frac{2h^2}{a^2(1+\nu)}\right) \text{ (bending)}$$

where a_3 and b_3 are evaluated using (11). The values of the hoop stress at the centre of a rotating solid shell are given in Table I for reference.

Results are presented in the following sequence. Firstly, we plot the stress concentration factor K_m, K_b and K_n as a function of the normalized bore radius r_b/r_c. Secondly, we present the hoop stress distribution along the radius for the optimal bore size. Finally, a

Table I
Hoop stress at the centre of a rotating solid shell

Shell thickness h (mm)	*Rim Radius r_c (mm)*							
	180.0		200.0		220.0		240.0	
	σ_m (*MPa*)	σ_b (*MPa*)	σ_m (*MPa*)	σ_b (*MPa*)	σ_m (*MPa*)	σ_b (*MPa*)	σ_m (*MPa*)	σ_b (*MPa*)
8	49.5	390.5	60.2	482.5	72.0	584.2	85.0	695.6
10	79.3	441.5	97.1	546.2	116.6	661.9	138.1	788.7
11	94.1	458.3	115.3	567.3	138.8	687.7	164.4	819.6
12	108.4	470.3	133.0	582.3	160.2	706.2	190.0	841.8

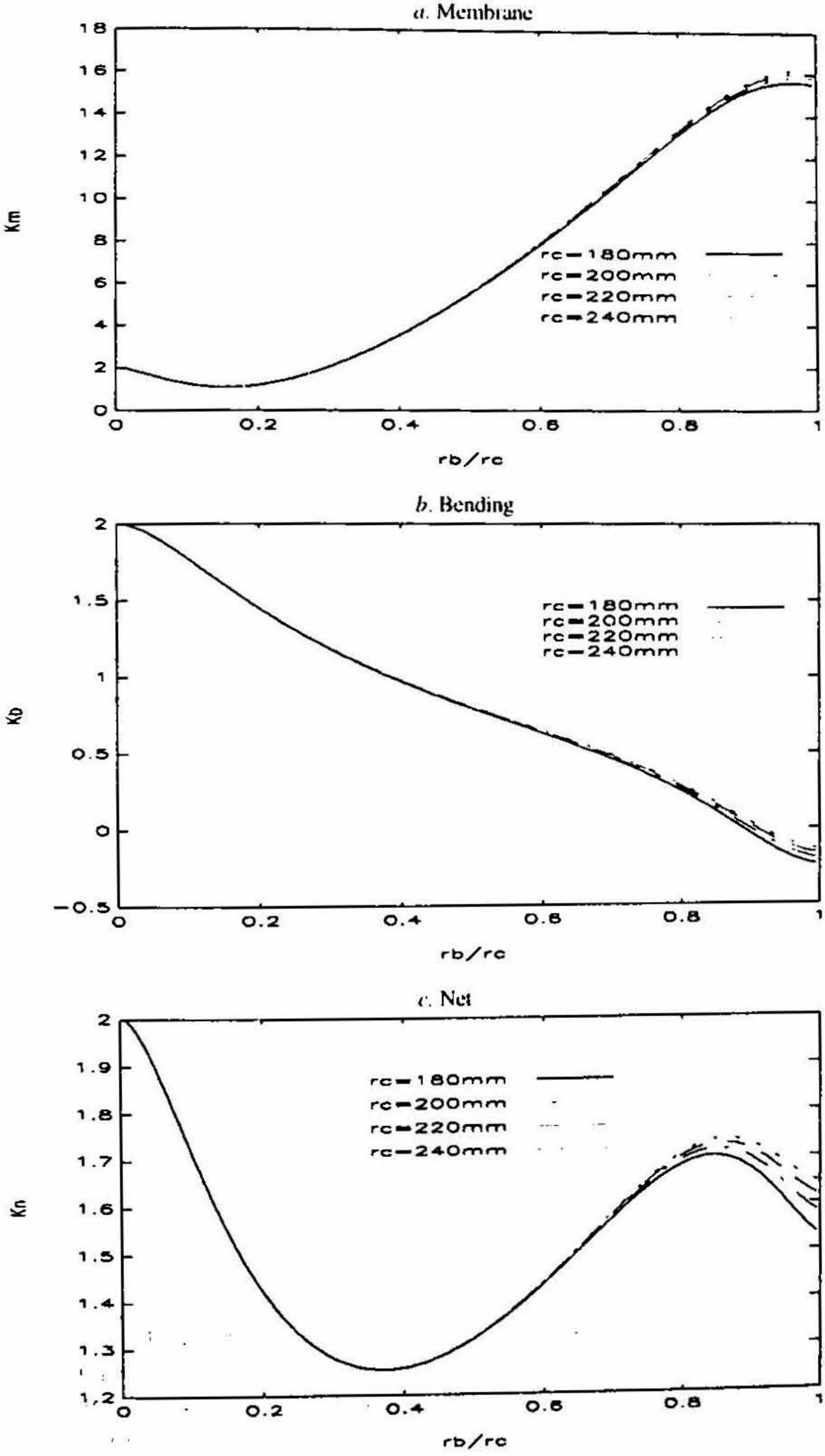

FIG. 4. Variation of stress concentration factor for 8 mm thick shell having sagitta 20 mm.

composite plot for the hoop stress distribution along the radius for the 11-mm thick shell is presented to demonstrate the uniformity of the hoop stress. This particular thickness of $h = 11$ mm represents the optimum design for the cases considered in this investigation. Further, nondimensional plots supplied here provide useful design guidelines for rotating hollow shallow shells.

Figure 4 shows the stress concentration factor for a shell of thickness 8 mm. The membrane effect is shown in Fig. 4a. The stress concentration factor K_m is 2 for a vanishingly small bore and decreases with the bore size initially before increasing again. The minimum value of K_m is registered approximately at a value of $r_b/r_c = 1/5$. Figure 4b shows the decreasing trend of K_b with bore radius. The net stress concentration factor K_n is shown in Fig. 4c. It is clear from this figure that the optimum bore size is $r_b/r_c = 0.37$.

Similar trends are observed for shell thickness of 10, 11 and 12 mm. In all the cases K_m attains its minimum around the same value of $r_b/r_c = 1/5$, but the minimum value of K_n is registered at increasing value of r_b/r_c. Thus, K_n is minimum at $r_b/r_c = 0.42$ when $h = 10$ mm; $r_b/r_c = 0.44$ for $h = 11$ mm; and $r_b/r_c = 0.47$ when $h = 12$ mm. It is also interesting to note that the minimum values of K_m and K_n remain approximately the same at 1.5 and 1.25, respectively, for all the cases studied here.

We now pursue the question of uniformity in the net hoop stress distribution along the radius of the optimized shell configurations. These configurations correspond to four different values of r_b/r_c for four different shell thicknesses considered in this study. The normalized values of the net hoop stress along the shell radius are shown in Fig 5 for different values of rim radii $r_c = 180$, 200, 220 and 240 mm. These plots reveal that when the shell thickness is 8 or 10 mm, the net hoop stress increases towards the rim. On the other hand, an opposite trend is noted for 12-mm thick shells. However, when the shell thickness is 11 mm there is little variation in the net hoop stress from the bore to the rim. This thickness, therefore, represents an optimum design. A composite plot of the net hoop stress distribution for $h = 11$-mm thickness shell for different rim radii is given in Fig. 6.

The results from this investigation demonstrate that the design of rotating shallow shell of constant thickness requires a careful study of the four geometrical parameters *viz.*, bore size (r_b), rim radius (r_c), thickness (h) and radius of the curvature of the shell (a). The shell height (sagitta) will be automatically fixed for a given combination of r_c and a. In the present study, the sagitta has been held constant at 20 mm, but a similar design procedure as outlined in this paper can be applied for other values of sagitta.

4. Conclusion

This investigation brings out the importance of an optimum bore size in the design of a rotating shallow shell. The design of high-speed rotating components such as turbine and compressor discs requires a careful selection of geometric parameters, *viz.*, thickness, rim radius and sagitta. The bending action significantly changes the optimization procedure based on minimizing the hoop stress at the bore. Discarding the bending effect suggests an optimum bore size of about 20% rim radius. Bending action makes it necessary to increase the bore size to as high as 50% of the rim radius. This may seem

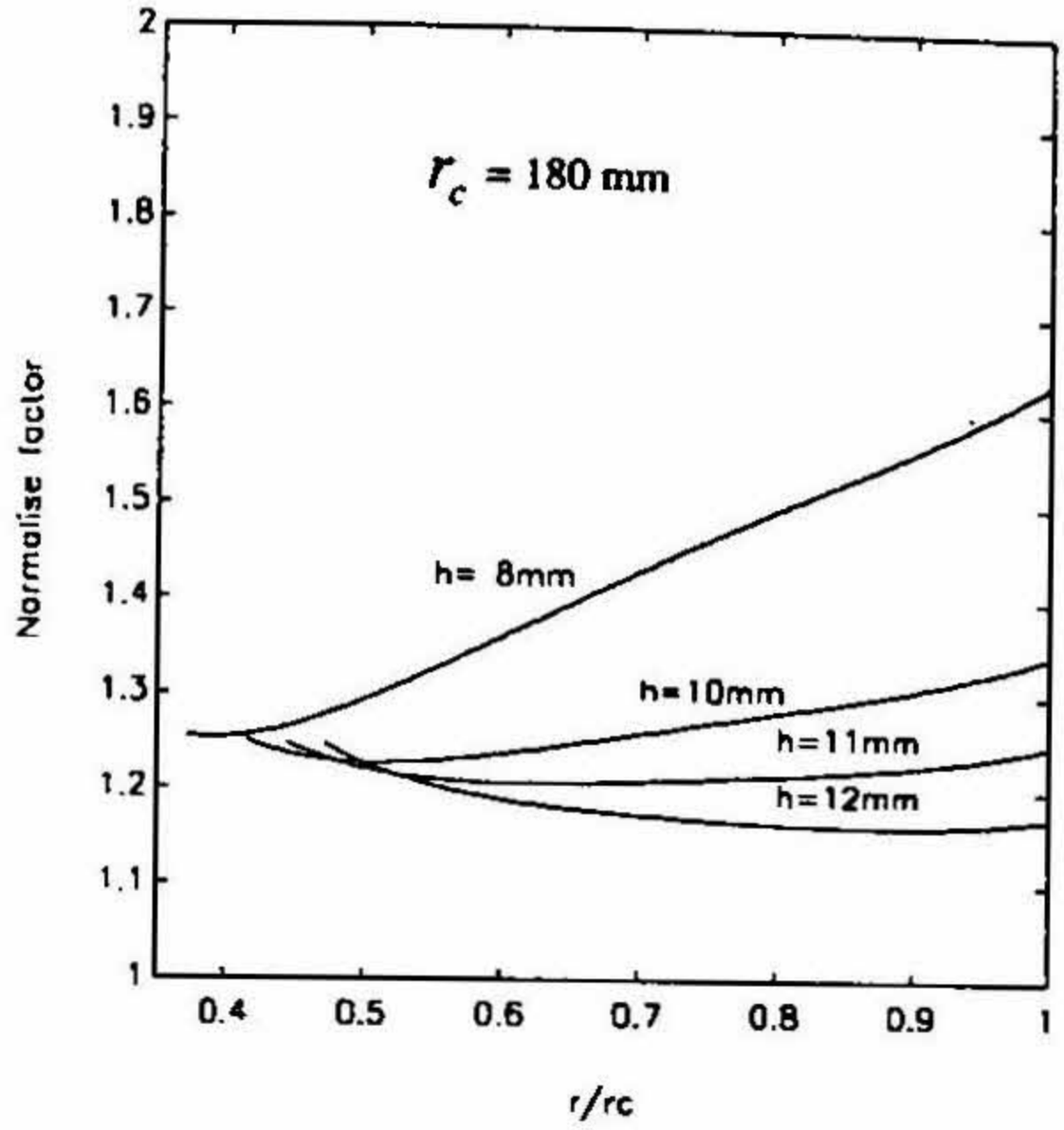

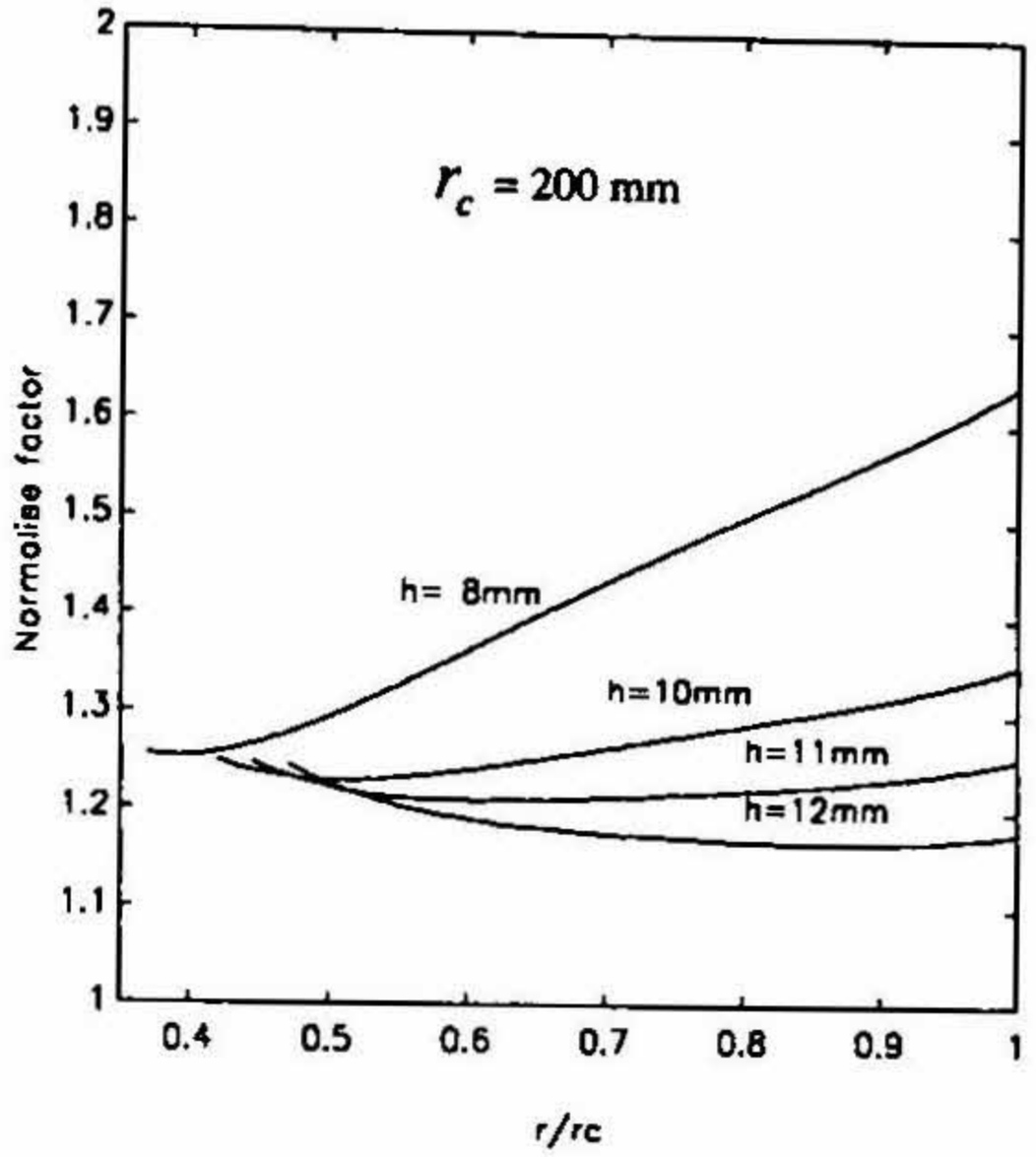

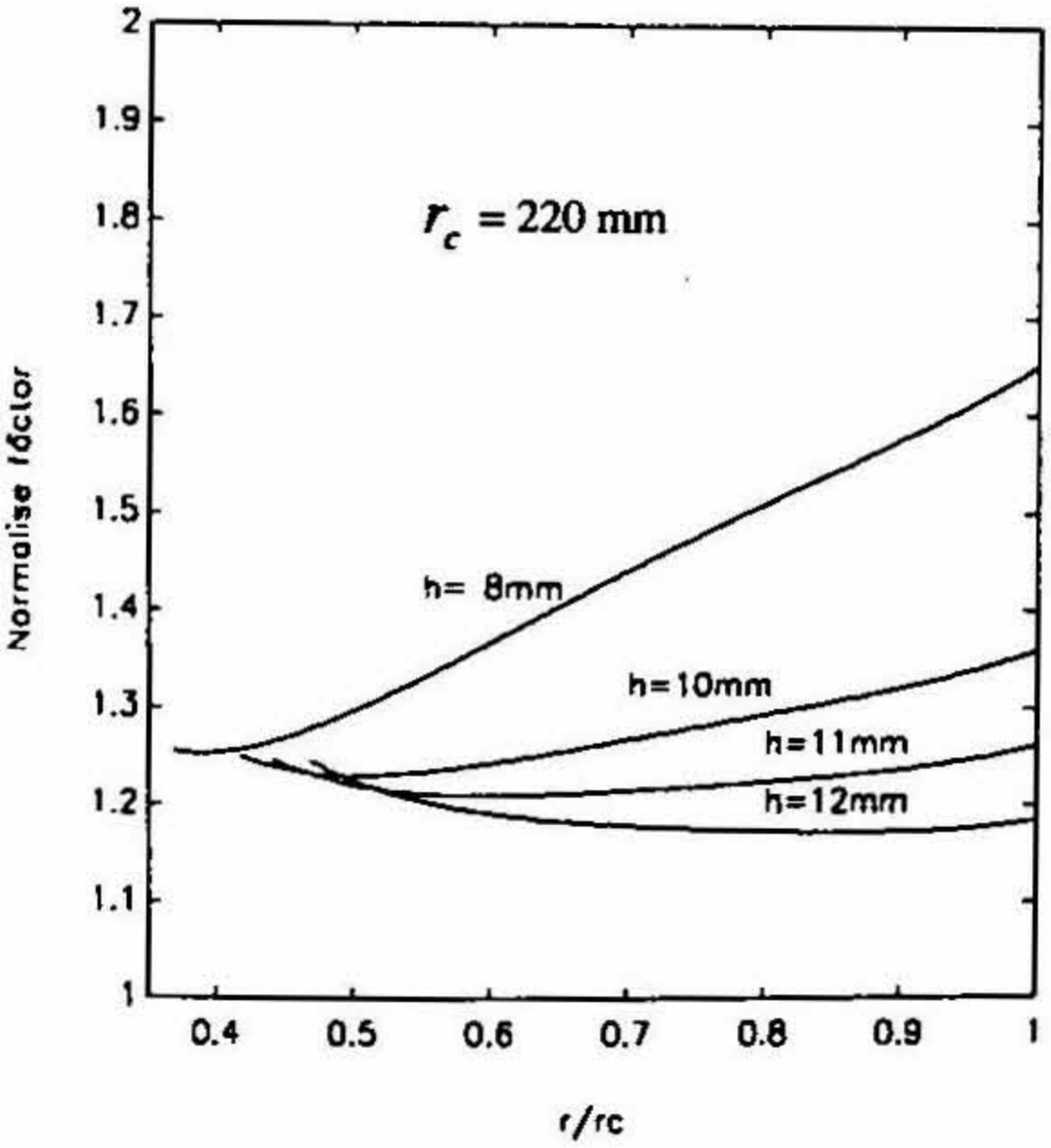

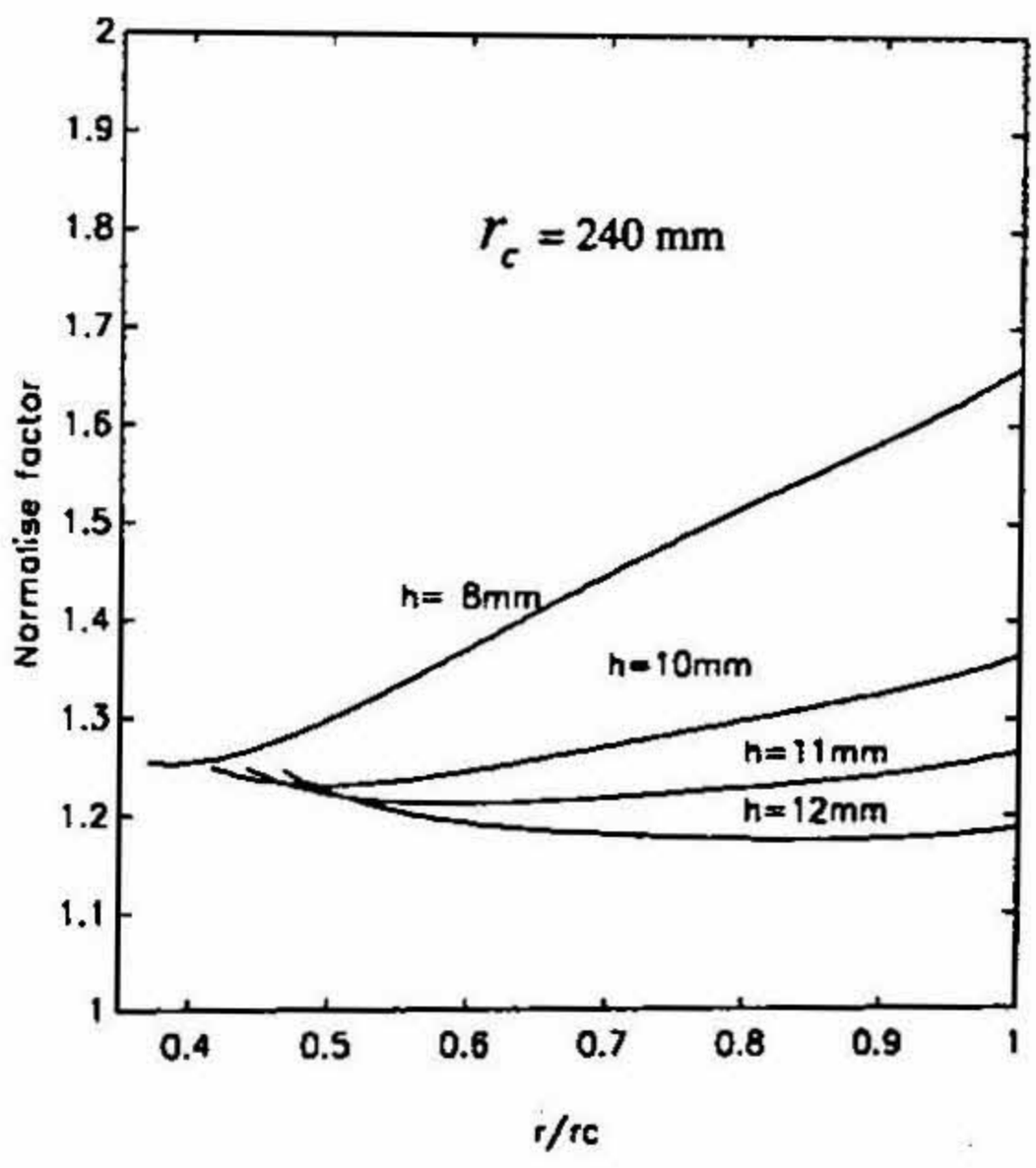

FIG. 5. Variation of the normalise values of the net hoop stress along the shell radius.

too large for practical implementation, and therefore it may become necessary to explore design optimization by using variable thickness shells to reduce the bore size. This aspect will be addressed to in a separate paper using the variable density approach developed by the authors. The new iteration scheme developed here can be rapidly implemented for design optimization prior to FEM validation of the prototype.

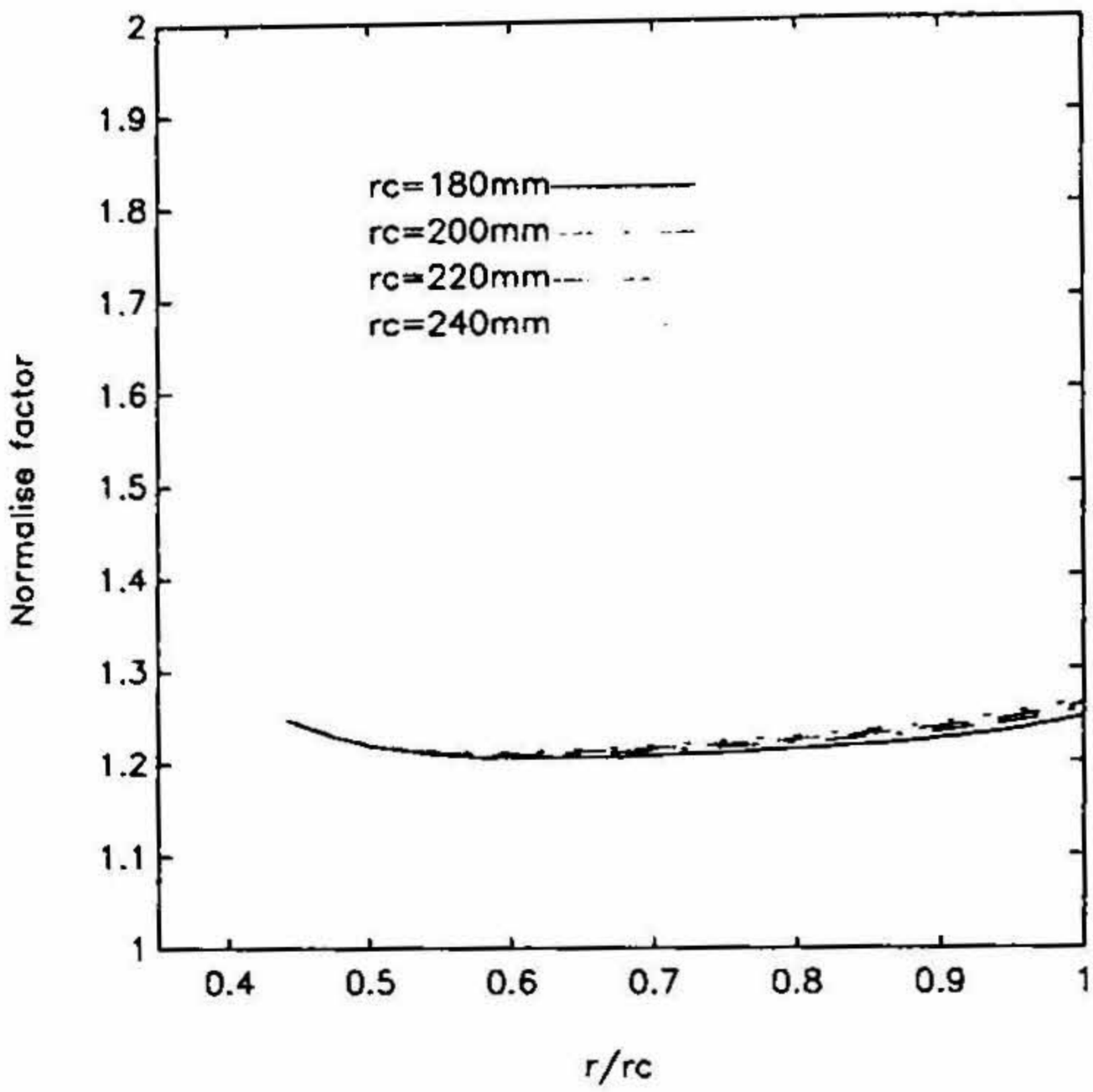

FIG. 6. Composite plot for normalise factor along the radius of the shell for he 11 mm thickness shell.

Acknowledgement

The authors are grateful to Dr R. Krishnan, Director, and Mrs N. Leela, Section Head, SWE(Engng), Gas Turbine Research Establishment, Bangalore, for their support and encouragement.

References

1. SIMHA, K. R. Y., RAJEEV JAIN, AND RAMACHANDRA, K. — Variable density approach for rotating shallow shell of variable thickness, *Int. J. Solids Struct.*, 1994, **31**, 849–863.
2. TIMOSHENKO, S. P. AND GOODIER, J. N. — *Theory of elasticity*, 3rd edn, p. 558, 1982, McGraw-Hill,
3. STODOLA, A. — *Steam and gas turbine*, Vol. 1, 1927, McGraw-Hill.
4. FLÜGGE, W. — *Stresses in shells*, 2nd edn, Ch. 5 and 7, 1973, Springer-Verlag.
5. TIMOSHENKO, S. AND WOINOWSKY-KRIEGER, A. — *Theory of plates and shells*, 2nd edn, p. 558, 1989, McGraw-Hill.
6. MCLACHLAN, N. W. — *Bessel functions for engineers*, p. 137, 1955, Oxford University Press.